Supplementary Information

Interior design of three-dimensional CuO ordered architectures with enhanced performance for supercapacitors

Jing Zhang,[a] Huijie Feng,[a] Qing Qin,[a] Guofeng Zhang,[a] Yingxue Cui,[a] Zhenzhen Chai[a] and Wenjun Zheng[ab]*

[a]Department of Chemistry, and Key Laboratory of Advanced Energy Materials Chemistry (MOE), TKL of Metal and Molecule-based Material Chemistry, College of Chemistry, Nankai University, Tianjin 300071, China. *E-mail: zhwj@nankai.edu.cn

[b]Collaborative Innovation Center of Chemical Science and Engineering, Nankai University, Tianjin 300071, China.

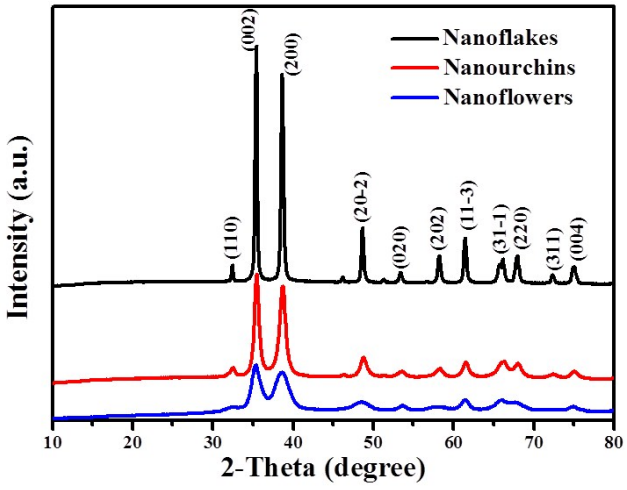

Fig. S1 XRD patterns of different CuO nanostructures.

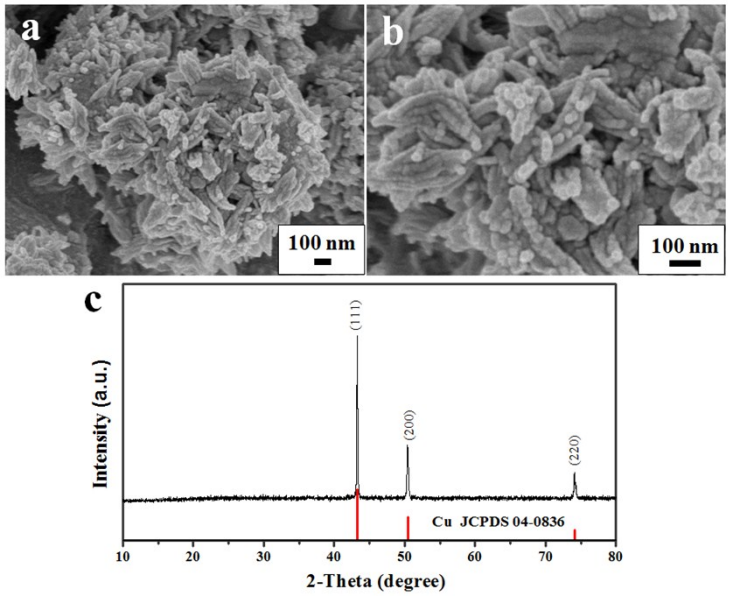

Fig. S2 a, b) SEM images and c) XRD pattern of the sample synthesized in pure EG.

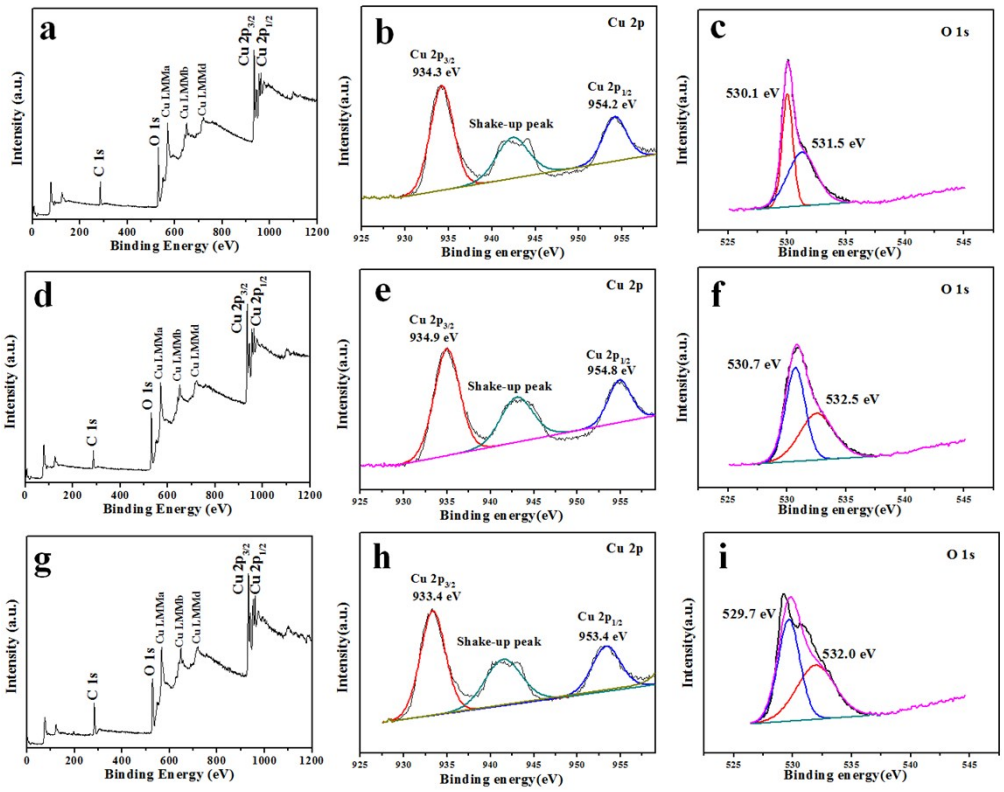

Fig. S3 Typical XPS spectra of three different nanostructures. CuO nanoflakes: a) survey spectra, b) Cu_{2p} region, and c) O_{1s} region; CuO nanourchins: d) survey spectra, e) Cu_{2p} region, and f) O_{1s} region; CuO nanoflowers: g) survey spectra, h) Cu_{2p} region, and i) O_{1s} region.

The survey XPS spectra indicates that the sample only contain Cu and O elements. The high-resolution XPS spectrum for the Cu 2p shows the binding energies of the Cu 2p3/2 and Cu 2p1/2 peaks at *ca.* 934 eV and 954 eV, respectively, which are typical values for Cu^{2+} in CuO.[36] The satellite peak at *ca.* 943 eV is evident of an open $3d^9$ shell, corresponding to shell Cu^{2+} state.[37] In addition, the fitted O 1s spectrum is characterized by two bands. The peak at about 530 eV is assigned to the CuO lattice oxygen, and the binding energy ~ 532 eV has been assigned in the literature to the presence of water.[36] Therefore, the obtained nanoflowers is pure CuO, which is consistent with the XRD result.

Table S1 The atomic ratios of Cu and O elements calculated from the XPS spectra.

	nanoflakes	nanourchins	nanoflowers
Atom% Cu	48.92	49.36	51.43
Atom% O	51.08	50.64	48.57

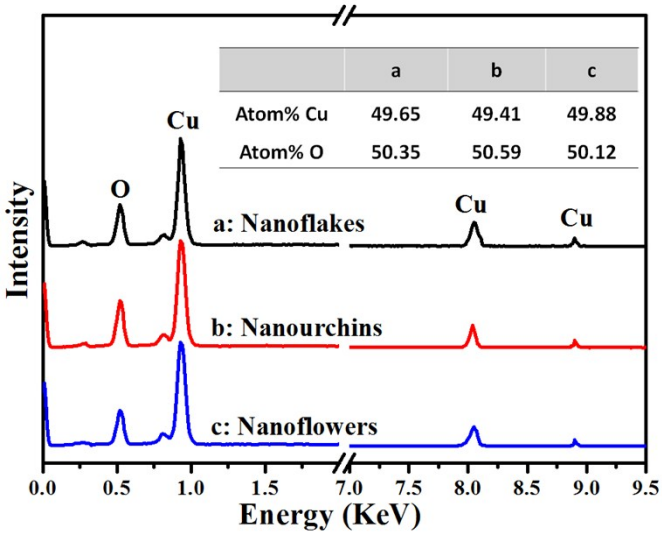

Fig. S4 EDS spectrum of different CuO nanostructures.

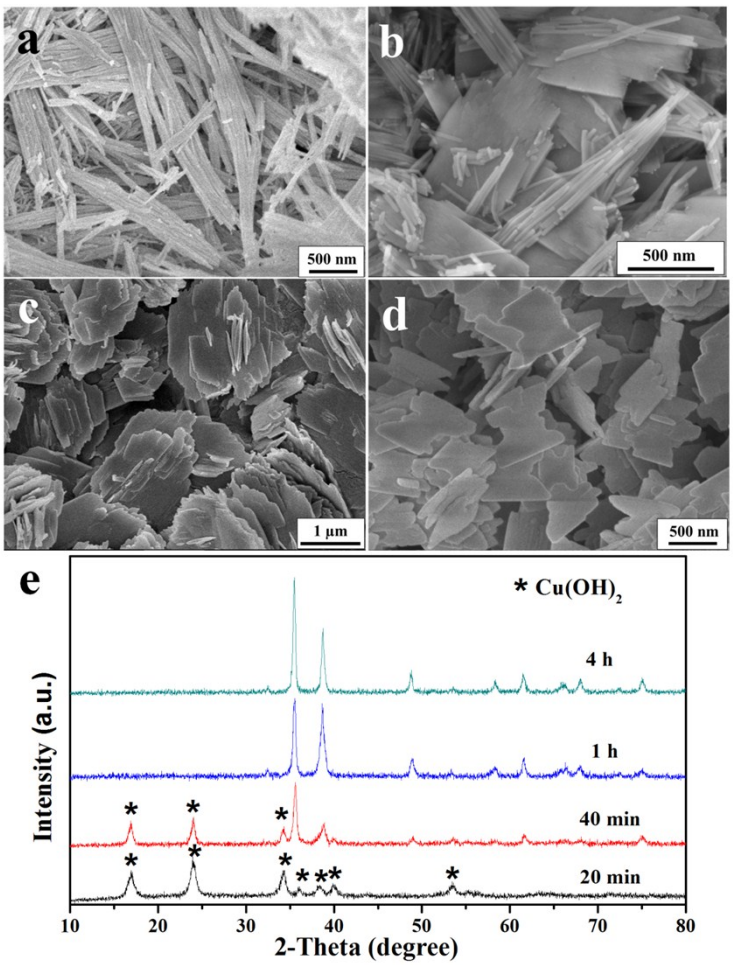

Fig. S5 a-d) SEM images and e) XRD patterns of CuO nanoflakes after different reaction time: a) 20 min; b) 40 min; c) 1 h; d) 4 h.

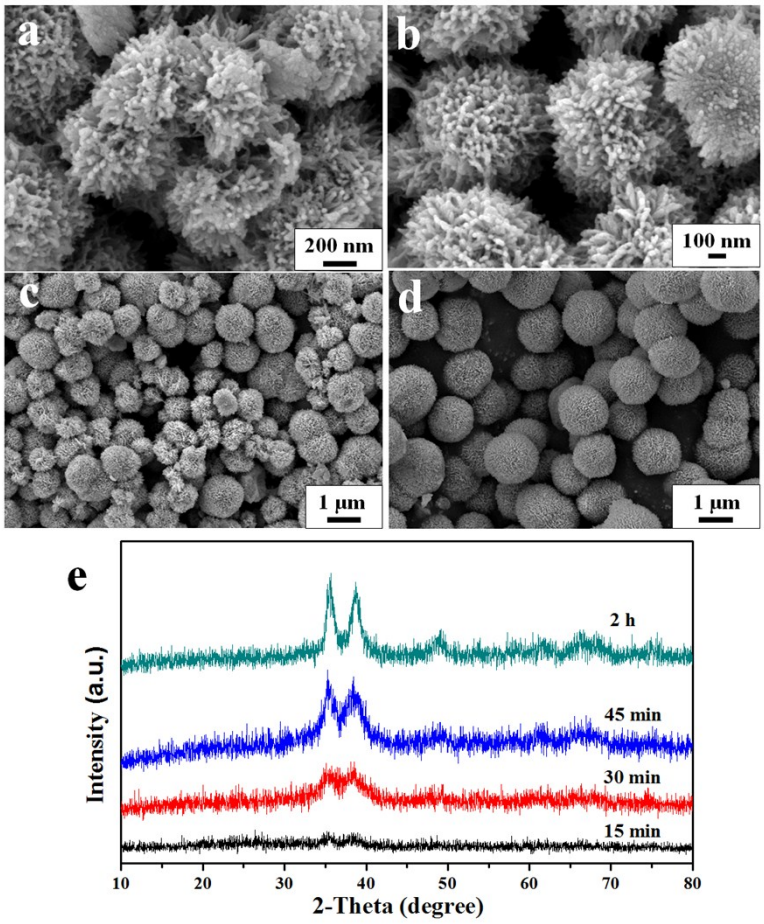

Fig. S6 a-d) SEM images and e) XRD patterns of CuO nanourchins after different reaction time: a) 15 min; b) 30 min; c) 45 min; d) 2 h.

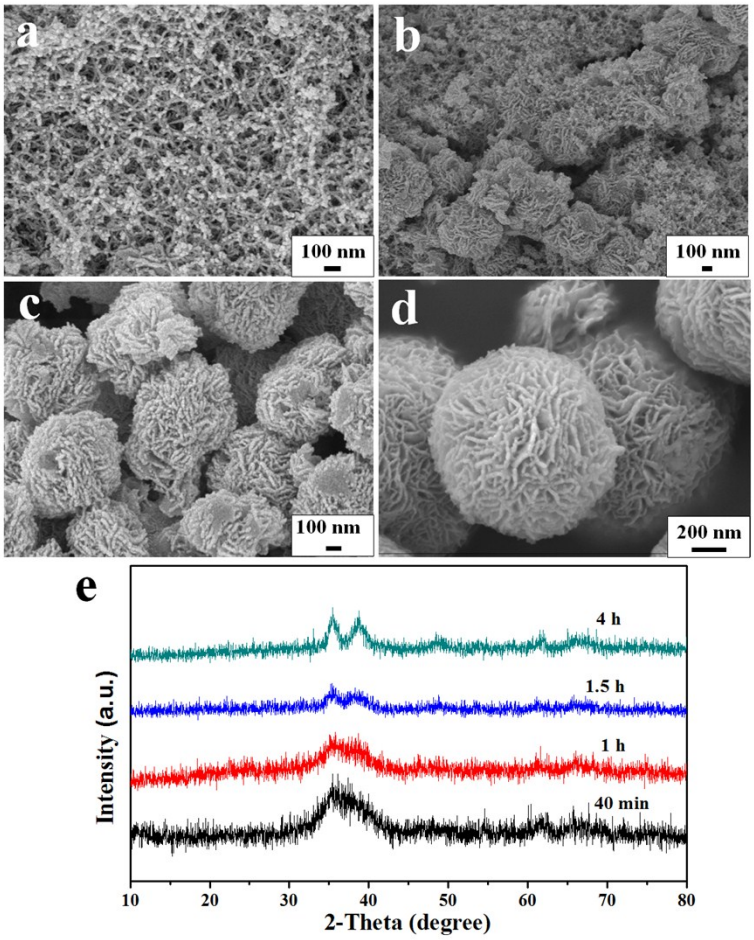

Fig. S7 a-d) SEM images and e) XRD patterns of CuO nanoflowers after different reaction time: a) 40 min; b) 1 h; c) 1.5 h; d) 4 h.

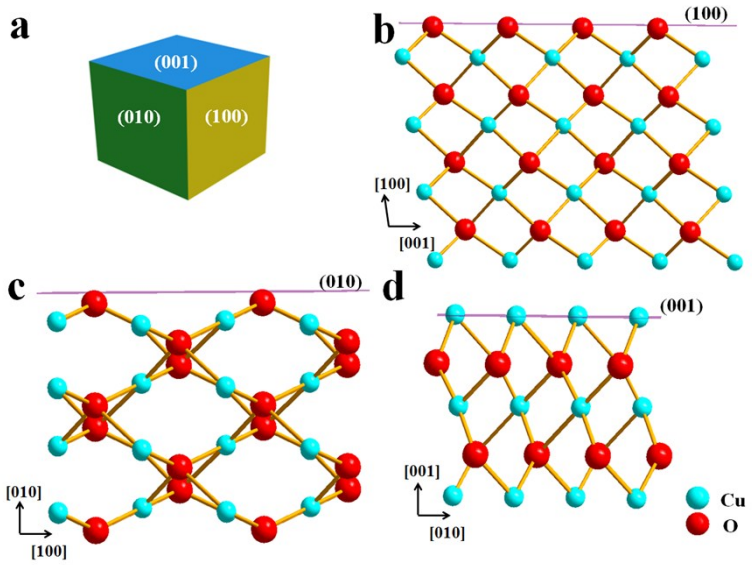

Fig. S8 a) A schematic of a CuO primary crystal, and b–d) atomic arrangements in (100), (010), and (001) planes, respectively.

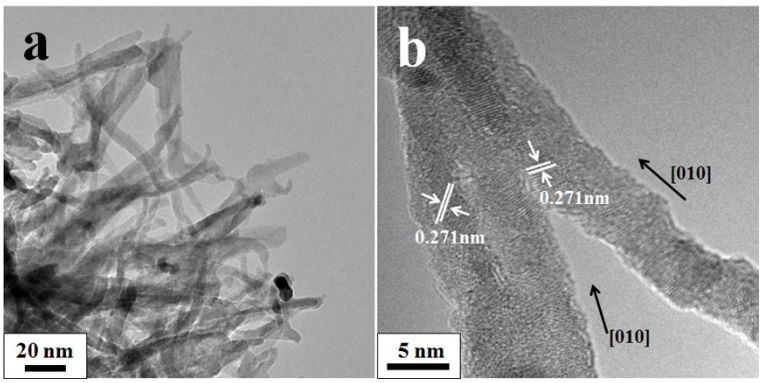

Fig. S9 a) TEM and b) HRTEM images of nanowires synthesized at 40 min during the formation of CuO nanoflowers.

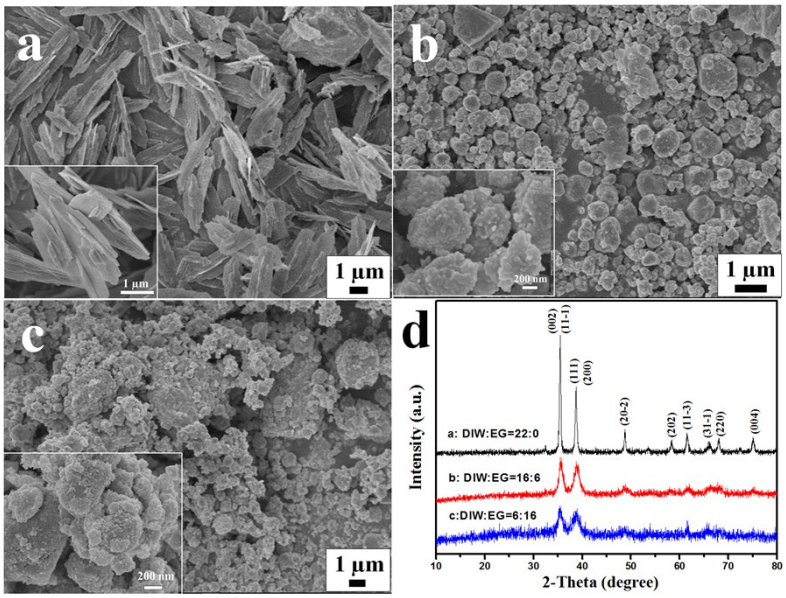

Fig. S10 SEM images and XRD patterns of the products prepared in different solvent by using NaOH instead of n-butylamine under the same pH values: a) DIW, b) V_{DIW} : V_{EG} = 16:6, c) V_{DIW} : V_{EG} = 6:16.

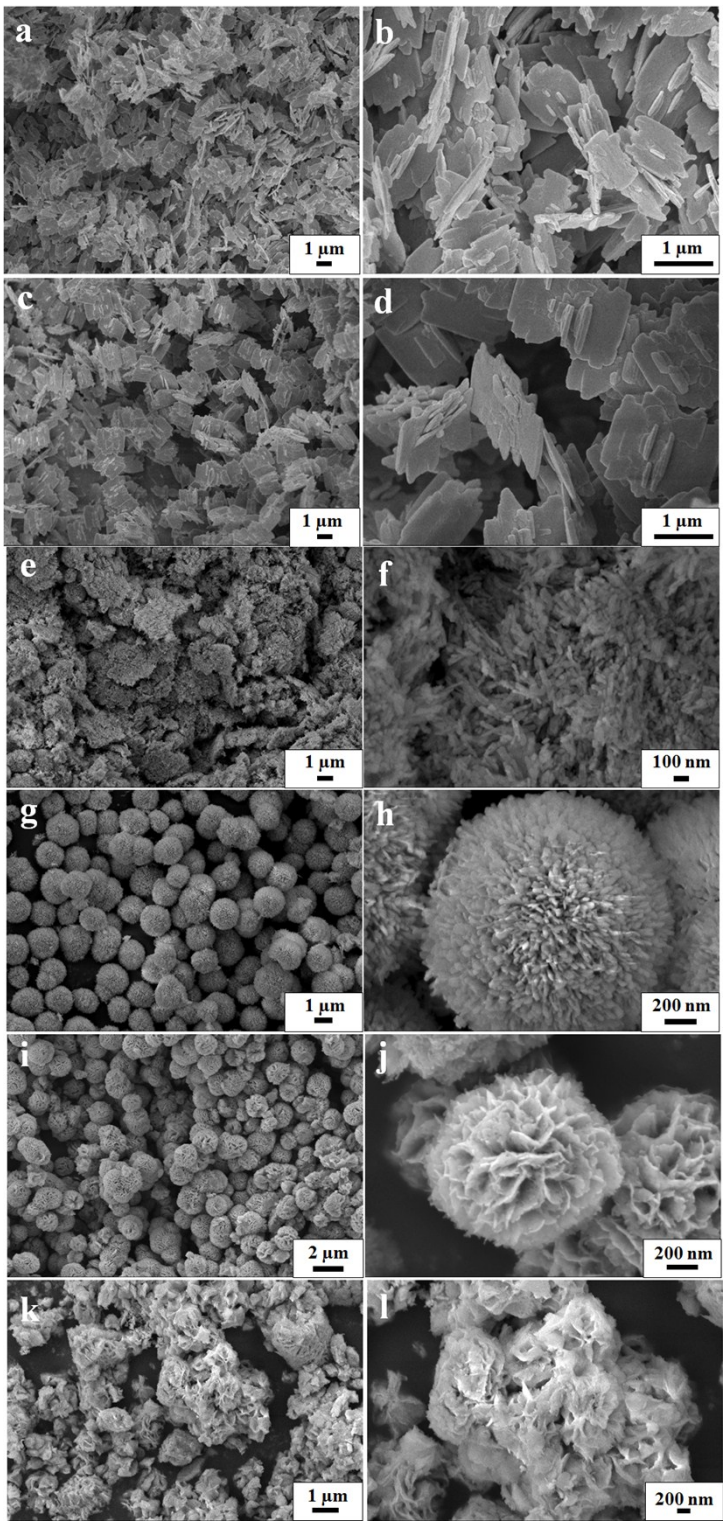

Fig. S11 SEM images of the products prepared by different solvent and content of *n*-butylamine: a, b) DIW, 0.5 mL; c, d) DIW, 4 mL; e, f) V_{DIW} : V_{EG} = 16:6, 0.5 mL; g, h) V_{DIW} : V_{EG} = 16:6, 4 mL; i, j) V_{DIW} : V_{EG} = 6:16, 0.5 mL; k, l) V_{DIW} : V_{EG} = 6:16, 4 mL.

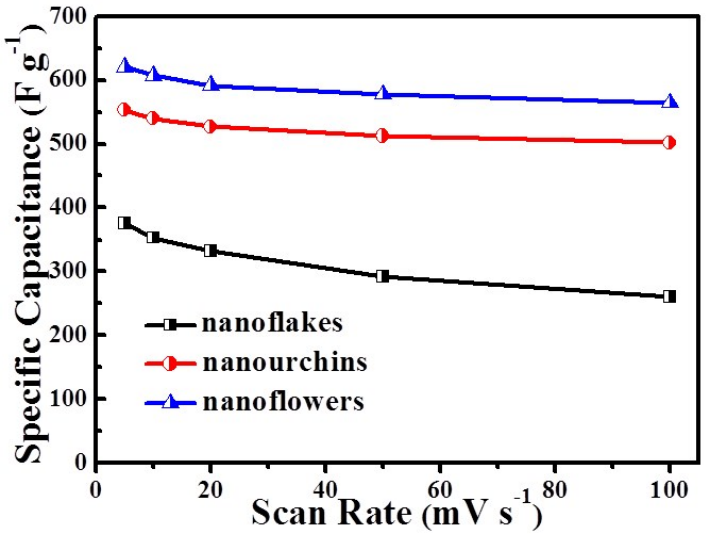

Fig. S12 Variation of specific capacitance versus scan rate for the CuO nanoflake, nanourchin, and nanoflower electrodes.

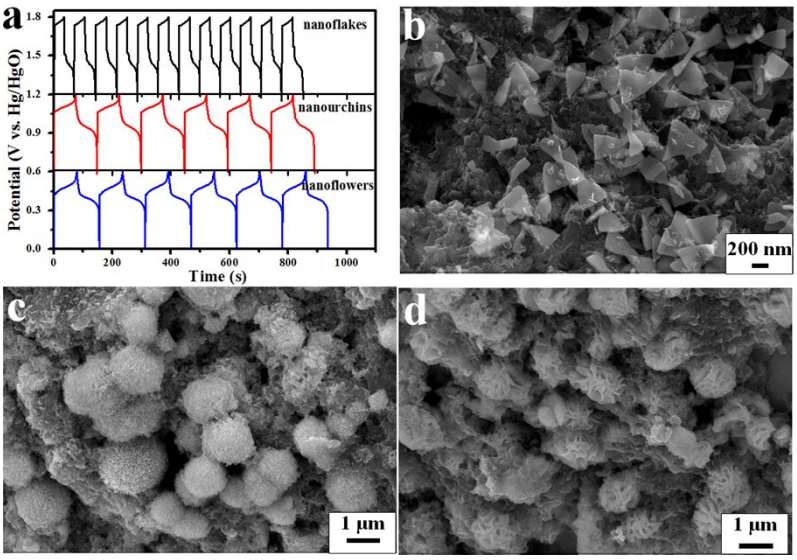

Fig. S13 a) The GCD curves of different CuO nanostructures after 8000 cycles, and SEM images of the active materials after 8000 charge-discharge cycles: b) nanoflakes; c) nanourchins; d) nanoflowers.

Table S2 The electrochemical performance of as-prepared 3D ordered CuO nanostructures compared with other CuO nanosturtures and other materials such as NiO, Co_3O_4, MnO_2, and RuO_2 using standard three-electrode system.

Material	Specific capacitance ($F\ g^{-1}$)	Stability	Electrolyte	Ref.
CuO nanobelts/CNT	151 (1 A g^{-1})	90% for 1000 cycles	1 M $LiPF_6$/EC:DEC	5
CuO nanowires	118 (1 A g^{-1})	No mention	2 M KOH	9
CuO nanosheets	346 (5 mV s^{-1})	85% for 5000 cycles	1 M Na_2SO_4	10
leaf-like CuO–graphene	331.9 (0.6 A g^{-1})	95.1% for 1000 cycles	6 M KOH	11
CuO 3D frameworks	431 (3.5 mA cm^{-2})	93% for 3000 cycles	3 M KOH	12
CuO gear-like structures	348 (1 A g^{-1})	87.9% for 2000 cycles	0.1 M KOH	13
CuO thin films	411 (5 mV s^{-1})	84% for 2000 cycles	1 M Na_2SO_4	14
CuO@C nanocomposites	207 (1 A g^{-1})	~100% for 1000 cycles	6 M KOH	S1
Porous C/NiO Nanocomposites	461 (2.3 A g^{-1})	83% for 1000 cycles	1 M KOH	17
Co_3O_4 porous polyhedron	504 (5 mV s^{-1})	No mention	6 M KOH	18
Reduced Co_3O_4 nanowires	977 (2 A g^{-1})	90% for 2000 cycles	1 M KOH	19
Aqueous MnO_2 ink	1035 (5 mV s^{-1})	No mention	0.5 M Na_2SO_4	20
Single-layer MnO_2 nanosheets	868 (3 A g^{-1})	91% for 10000 cycles	1 M Na_2SO_4	21
RuO_2 nanoparticles anchored graphene and CNT hybrid foam	503 (1 mA cm^{-2})	106% for 8100 cycles	2 M Li_2SO_4	S2
CuO nanourchins CuO nanoflowers	541 (1 A g^{-1}) 585 (1 A g^{-1})	85.3% and 86.8% for 8000 cycles	3 M KOH	This work

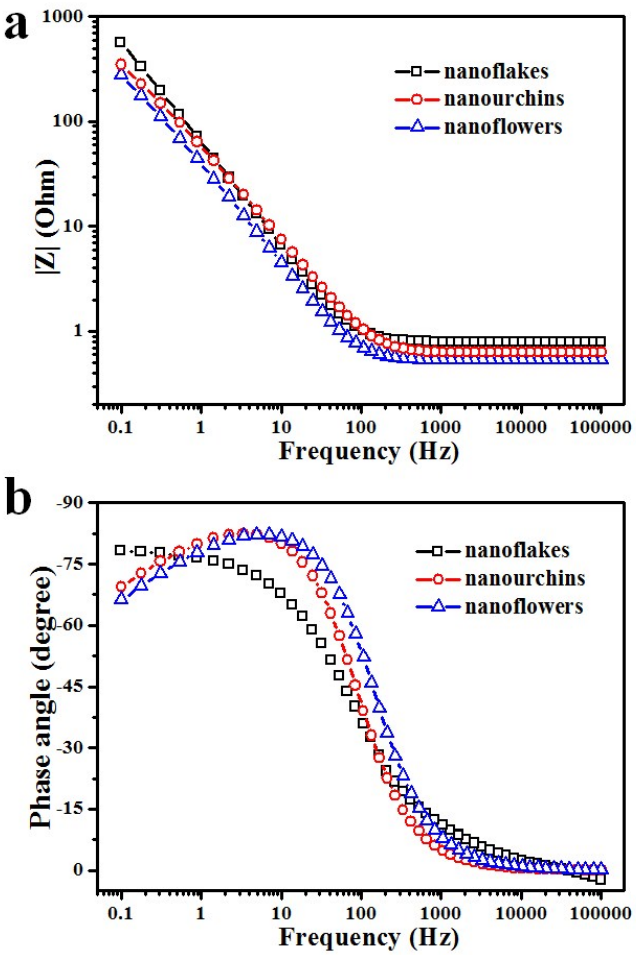

Fig. S14 a) Magnitude vs. frequency plots and b) Bode phase of different CuO electrodes.

Table S3 Internal resistance (Rs) and charge transfer resistance (Rct) of different CuO nanostructures after 1 and 8000 charge–discharge cycles.

	nanoflakes	nanourchins	nanoflowers
R_s (1 cycling)	0.632 Ω	0.293 Ω	0.268 Ω
R_{ct} (1 cycling)	0.464 Ω	0.157 Ω	0.150 Ω
R_s (8000 cycling)	1.963 Ω	0.375 Ω	0.347 Ω
R_{ct} (8000 cycling)	1.410 Ω	0.171 Ω	0.163 Ω

Ion diffusion calculation.

Diffusion flux is determined by Fick's first law as following equation.

$$J = -D\frac{dc}{dx}$$

where J is diffusion flux, D is diffusion coefficient. J is proportional to concentration gradient. Diffusion coefficient is related to the mobility of the diffusion ions and is proportional to the squared velocity of diffusing ions, which means the faster diffusion of ions with higher diffusion coefficient. The electrochemical impedance spectroscopy (EIS) can be used to estimate ion diffusion at electrode surface. The straight spot of the imaginary impedance against the real impedance in the low-frequency region indicates the ion diffusion controlled system due to the fractal geometry effects on the electrode surface.[S3,S4] Therefore, the Warburg impedance (Z_w) from a semi-infinite diffusion of ions can be evaluated as follow: [S3]

$$Z_w = \sigma\omega^{-1/2}\ (1-j) \qquad (1)$$

where σ is the Warburg coefficient and ω is the angular frequency. It can be seen that the linear plot of the real (Z') or imaginary (Z'') part against the angular frequency ($\omega^{-1/2}$) determines the Warburg coefficient (σ) value from the slope of the plot, as shown in Fig. 5d. The diffusion coefficient (D) of electrolyte ions at the interfacial region is calculated according to the following equation 2:[S4]

$$\sigma = \frac{RT}{n^2F^2A\sqrt{2}}\left(\frac{1}{D^{1/2}C^*}\right) \qquad (2)$$

where R is the gas constant, T is the absolute temperature, n is the charge-transfer number, A is the area of the electrode surface, and C^* is the electrolyte concentration.

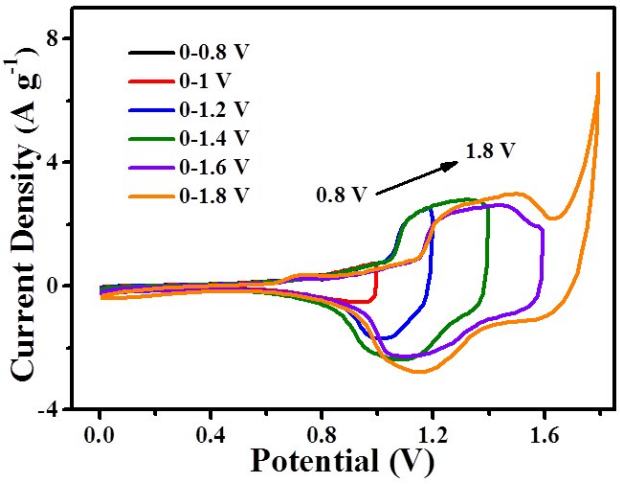

Fig. S15 CV curves of the CuO nanoflowers//AC asymmetric supercapacitor within different potential windows at a scan rate of 50 mV s^{-1}.

References

S1 T. Wen, X. L. Wu, S. W. Zhang, X. K. Wang and A. W. Xu, *Chem. Asian J.,* 2015, **10**, 595.

S2 W. Wang, S. R. Guo, I. Lee, K. Ahmed, J. B. Zhong, Z. Favors, F. Zaera, M. Ozkan and C. S. Ozkan, *Scientific Reports,* 2014, **4**, DOI: 10.1038/srep04452.

S3 R. P. Janek, W. R. Fawcett and A. Ulman, *Langmuir,* 1998, **14**, 3011.

S4 C. -T. Hsieh, S. -M. Hsu, J. -Y. Lin and H. Teng, *J. Phys. Chem. C,* 2011, **115**, 12367.